Chapter 4

Rain Drop Size Distribution and Variation of Attenuation With Rain Fall Rate

4.1 DISDROMETERS

Disdrometers are one of the most common tools used to measure rainfall rate and raindrop size distributions. There are several types of disdrometers available including optical, impact and video disdrometers. Video disdrometers have been shown to have better agreement with rain gauge measurements of rainfall rates in comparison to impact disdrometers [60]. Both disdrometers partially underestimate rainfall rate by underestimating the number of smaller size raindrops. However, the video disdrometer had a better estimate of the number of small size drops.

Figure 4.1. Images of video (left), optical (center) and impact (right) disdrometers

A Joss-Waldvogel (impact) disdrometer measures the size and number of raindrops by the vibrations caused by each impact on the surface of the disdrometer. It is typically constructed of a conical Styrofoam body used to transmit the mechanical impulse, caused by vibrations, to two moving coils. A drop lands on the surface of the disdrometer and the resulting mechanical movement induces a voltage across the sensing coil. This voltage is processed to convert the vertical momentum of a raindrop into an electronic pulse that is proportional to the drop diameter [61]. The voltage is also amplified and applied to the drive coil to counteract the movement. This limits the movement so the device is quickly ready for the next drop. A Joss-Waldvogel disdrometer typically measures the number and size of raindrops over 128 bins at ten second intervals. The disdrometer has a measurement range of 0.3mm to 5.0mm raindrops. Drops smaller than 0.3mm hold little significance when considering radio wave attenuation and drops greater than 5.0mm are very rare as they are hydro dynamically unstable.

There are several disadvantages when measurements are made by disdrometers in gen- eral, as discussed by Brawn and Upton in 2008[61]. Each disdrometer has a minimum drop size it can measure, which can bias the results. Similarly, disdrometers can have a maximum measurement size, which would result in the largest drops being measured incorrectly. Each disdrometer has a relatively small collection area, which makes drop counting for each diameter class noisy, especially in the case of larger drops. Optical disdrometer measurements may be effected during heavy rain when one drop may be obscured by another. Joss-Waldvogel disdrometers can be subject to noise caused by strong winds, high acoustics (in the case of an impact disdrometer), splashing drops or debris landing on the device. Further, impact disdrometers may exhibit a 'dead-time' caused by the impact of a drop, during which small drops cannot be measured. Despite the disadvantages of the optical disdrometer, the device is a very good measure of raindrop size, which is cheaper, more widely available and has an abundance of data when compared to a video disdrometer.

In this work OTT Parsivel optical disdrometer is used to obtain DSD data, at KLUniversity(16.5083° N, 80.6417° E), Guntur. Rain events are recorded by using the OTT Parsivel2 laser optical disdrometer which is a modern, laser-based disdrometer for comprehensive and reliable measurement of all types of precipitation. It measures precipitation particles using shadowing effects of particles passing through the laser strip and the extinction principle. Parsivel2 captures both the size and the falling rate in detail of the individual hydrometeors and classify them into a range of 32 size and 32 velocity classes. Depending on the data recording interval the resulting precipitation spectrum uses either 10 seconds or1 minute or one hour Internal. Data processor uses the recorded raw data to measure the type of particle and amount of precipitation for a given interval of time, also the MOR visibility, kinetic energy of the precipitation and the equivalent radar reflectivity. Using standard ports, both the calculated and the spectral data are output to a data logger, an automatic weather station or a PC.

In order to investigate the DSD number of analytical forms of rain drop size distributions have been suggested. These include the exponential distribution or Marshall and Palmer distribution [63], lognormal distribution [64], the gamma distribution [65] and the normalized gamma distribution [66].

4.2RAINDROP SIZE DISTRIBUTION

The raindrop size distribution (DSD), denoted by N(D), is the number concentration of raindrops with equivolume diameter D in a given volume of space (number of drops m^{-3} mm^{-1}). DSDs can be used to calculate rainfall rate and radio wave attenuation. The DSDs can vary significantly and yet give the same rainfall rate. For instance, a large number of small drops can give the same rainfall rate as a small number of large drops, even though they are two very different raindrop size distributions. Two different DSDs resulting in the same rainfall rate may result in two different values of signal attenuation.

4.2.1 Laws and Parsons Distribution Model

This model is the best-known drop size distribution model and is recommended by the ITU-RP 838 (2005) for the calculation of specific attenuation of slant path [71]. This distribution was developed experimentally by using rudimentary technique (Laws and Parson, 1943). It was concluded that the actual drop size distribution on the terminal ground can be obtained from the terminal fall velocity V(a), and volume distribution is given as.

$$\mathbf{N(D) = \frac{10^3 R\beta(m)dD}{4.8\pi D^3 v(D)}} \qquad (4.1)$$

4.2.2 Exponential Distribution

The first significant work on raindrop size distributions started with Laws and Parsons in 1943 and continued with Marshall and Palmer in 1948. Marshall and Palmer measured raindrops on dyed filter paper to analyze the distribution of drop sizes. With the results obtained, Marshall and Palmer derived the general relation

$$\mathbf{N_v(D) = N_0 exp(-\Lambda D)} \qquad (4.2)$$

where $\Lambda(mm^{-1})$ is drop size distribution slope factor which is the inverse of rain drop mean diameter present in a volume of air[14],[15], $N_0(mm^{-1}m^{-3})$ is drop size distribution for D=0, Marshall and palmer found that N_0 was approximately constant for any rain rate[3].

$$\mathbf{N_0 = 8.0 * 10^3} \quad (4.3)$$

slope factor Λ decreases with the increase of Rain rate R and is given by

$$\mathbf{\Lambda = 4.1 R^{-0.21}} \quad (4.4)$$

Where R is the rainfall rate in mmhr^{-1}. The Marshall and Palmer distribution of raindrops with size is shown in Figure 4.2 for 0.25, 1, 5, 25 and 150mmhr^{-1}. Major limitation of this method is it overestimates the drop distribution for smaller rain rates that is when drop size is less than 1 to 5mm but in the tropical environment because of convective type of rain usually the rain intensities are very high with large drop diameter. The Marshall and Palmer DSD have been widely accepted by many, and is a good representation of the DSD over a long time period.

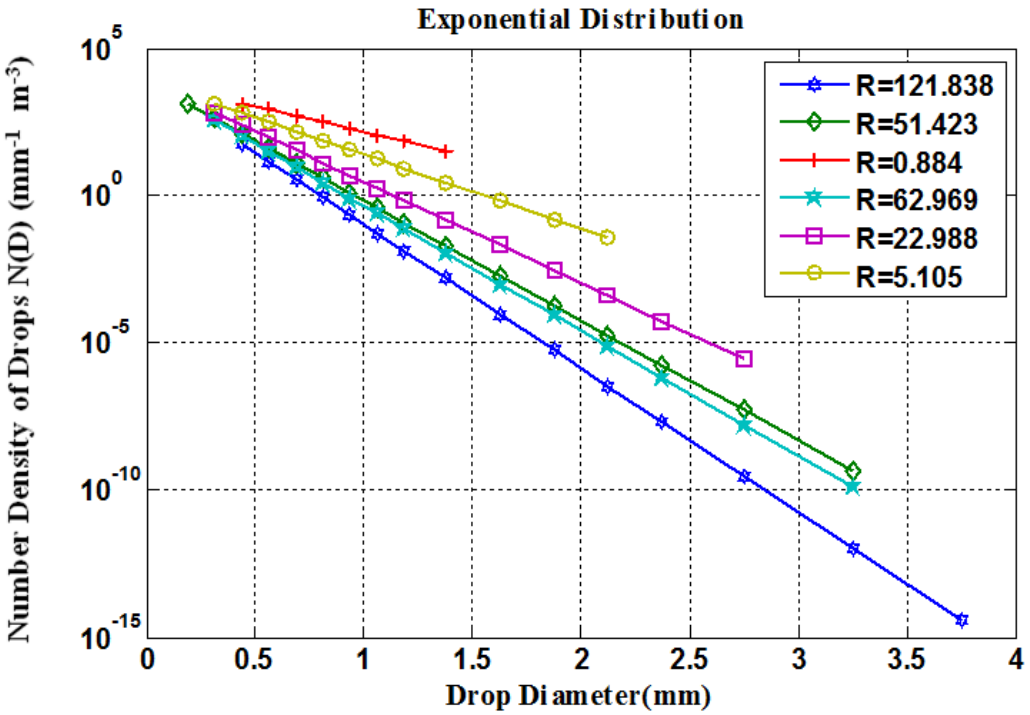

Figure 4.2:Exponential drop size distribution for various rain events

From the figure 4.2 drop size varies between 0.5mm to 1.5mm when the rainfall rate R=0.884mm/h, drop size varies between 0.3 to 2.2mm for rain fall rate R=5.105mm/h, drop size varies between 0.3mm to 2.8mm for rain fall rate R=22.988mm/h, drop size varies between 0.2mm to 3.3mm for rain fall rate R=51.423mm/h, drop size varies between 0.3mm to 3.35mm for rain fall rate

R=62.969mm/h, drop size varies between 0.5mm to 3.8mm for rain fall rate R=121.838mm/h.

4.2.3 Log-Normal Distribution

An alternative representation of the DSD is the lognormal distribution, shown in Figure 4.3. The lognormal distribution can better estimate DSDs where there are fewer numbers of small drops sizes, i.e. for convective rain. Comparing Figures 4.2 and 4.3 shows that the lognormal distribution has more versatility in representing different DSDs for a given rainfall rate is given in equation (4.5). The lognormal distribution can represent instances of DSDs with few small drops, for example the distributions shown in Figure 4.3, to instances that with high numbers of small drops, which are more exponential in shape[64]. lognormal distribution is a better fit to observed DSD data in several tropical places compared to exponential and gamma distributions [64].

$$N(D) = \frac{N_0}{\sqrt{2\pi\sigma D}} e^{\frac{\ln(D-\mu)^2}{2\sigma^2}} \quad (4.5)$$

Where $N_0 = 108R^{0.363}$, R is the rain rate in mm/h, D is the diameter of rain drop in mm, σ is the standard deviation.

$$\mu = 0.01709\log(R^2) + 0.1108\log(R) + 0.2705 \quad (4.6)$$

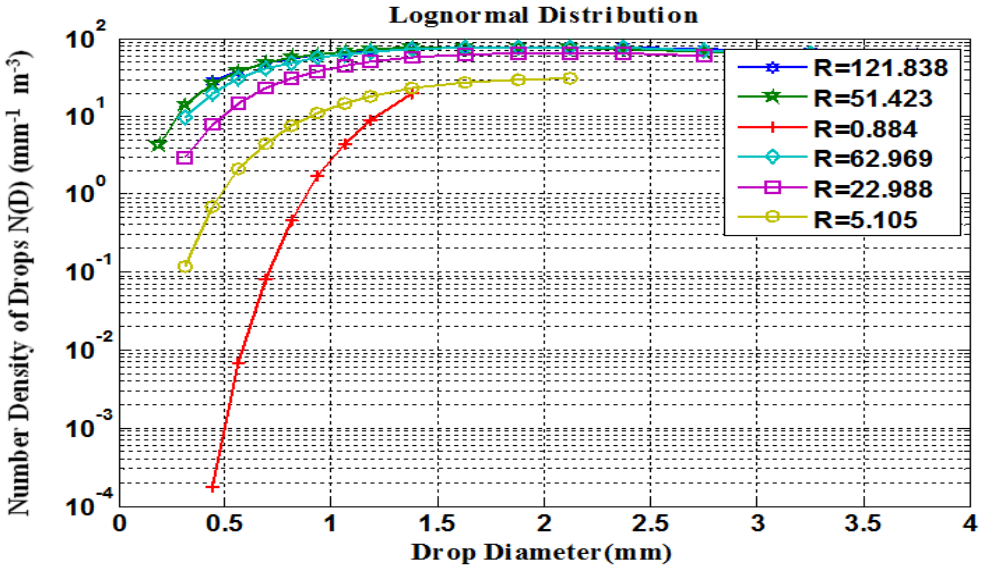

Figure 4.3: Log normal drop size distribution for various rain events

4.2.4. Gamma Distribution

The gamma distribution also presents N (D) directly, but in contrast to the negative exponential, when approaches to zero it correct the exponential increase of the raindrop number per unit volume when D tends to zero. It is two parameter exponential distribution, which does not restrict N_0 to a fixed value as in above model and the model is represented as

$$N(D) = N_0 D^{\mu} e^{-\lambda D} \quad (4.7)$$

$$N_0 = e^{(0.04533 \log(R^3) - 0.4187 \log(R^2) + 1.48 \log(R) + 4.929)} \quad (4.8)$$

$$\mu = 0.01709 \log(R^2) + 0.1108 \log(R) + 0.2705 \quad (4.9)$$

$$\lambda = 4.1 R^{0.21} \quad (4.10)$$

And D is the rain drop diameter in mm, R is the rain rate in mm/h.

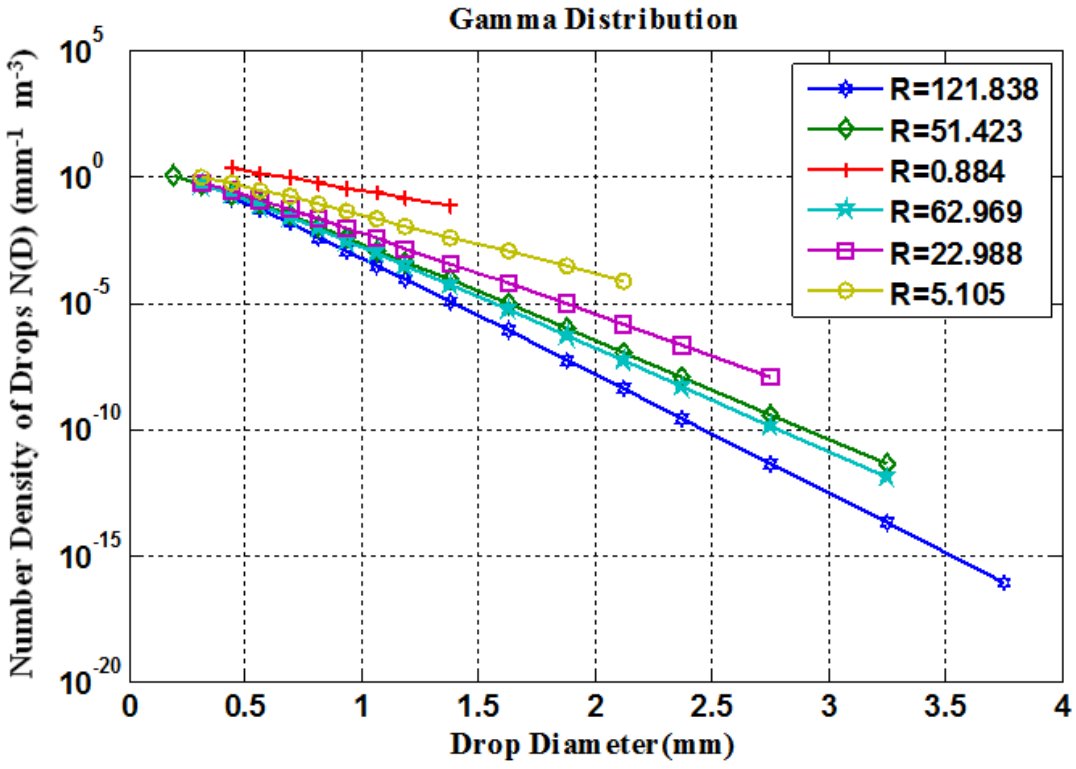

Figure 4.4 Gamma drop size distribution for various rain events

Gamma distribution is the best suitable for the tropical environment which has convective type of rain fall with heavy intensity as well as for low rain falls also. Exponential distribution is the special case of gamma distribution when μ is zero for all other values it will be the gamma distribution.

4.3RAIN FALL RATE

Rainfall rate is a measure of the amount of rain precipitation over a given time ($mmhr^{-1}$) and is a function of the raindrop size distribution. Rainfall rate, as given by Baltas and Mimikou in 2002[61], can be defined by the following equation (4.11)

$$\mathbf{R} = \frac{\mathbf{3.6}}{\mathbf{10^3}} \frac{\boldsymbol{\pi}}{\mathbf{6}} \int_{\mathbf{0}}^{\infty} \mathbf{v(D)D^3N(D)dD} \qquad (4.11)$$

Where R is the rainfall rate, v (D) is the fall velocity of the drop at diameter D and N (D) is the raindrop size distribution.

Rainfall rate is proportional to the moment of N(D, t), the measured DSD at the discrete instant t (time in seconds), of order 3.67[102]. The fall velocity (v(D)) may be assumed to be $v(D) = 3.78 * D^{0.67}$ as proposed in Atlas and Ulbrich in 1977[101]. The general expression of the n^{th} order moment of the raindrop size distribution is given in equation (4.12):

$$\boldsymbol{m_n(t) = \int_0^{\infty} D^n N(D,t).dD = \sum_{i=1}^{n_c} Di^n . N_m(D_i,t).\Delta Dt} \qquad (4.12)$$

The following equation shows rainfall rate proportional to the moment of the raindrop size distribution of order 4.13:

$$\boldsymbol{R = 3.78.\frac{\pi}{6} . m_{3.67}(t)} \qquad (4.13)$$

Rainfall rate can be measured over different time intervals. During a long time interval (an hour or more) a rain event may change considerably. Measuring rainfall rate over such a long time period effectively averages the rainfall rate. Small time intervals (such as 1 minute) will represent more changes in the rain event, which is discussed further in this Chapter.

4.4 DISDROMETER USED IN THIS WORK

OTT parsivel disdrometer was used to measure DSD in this work at KLUniversity(16.44^{o} N,80.62^{o}E) over 2 and half years from june2012-december 2014.The raindrop size distribution from disdrometer can estimated using the three methods discussed in the section 4.2.DSD calculated for various rain events with different rain rate values with different integration periods usually in this work all the recordings with 10s interval.

4.4.1 Disdrometer integration time interval

The disdrometer measures the number and size of raindrops over ten second intervals. The data is accumulated to produce a time interval of one minute. This period balances uncertainty in the estimation of DSD parameters from measurements taken against the dynamics of the rain event. In Figure 4.5 to 4.7 DSDs determined from the disdrometer are illustrated for different time integration periods with three model like exponential, lognormal and gamma. Long integration periods (e.g., one hour) reduce the uncertainty in estimating the DSD parameters but may not represent well the dynamics of rain events. Conversely, short integration periods (e.g., 10 seconds) may not yield sufficient samples to reliably estimate the DSD parameters, especially at low rainfall rates. The number of instances of large raindrops is relatively low due to the formation process of raindrops. Therefore, only longer time periods may obtain enough samples to effect the DSD for larger raindrops. To capture the dynamics of intense convective rain events, which may last only a few minutes, one-minute integration time was selected (unless otherwise stated) as a compromise between uncertainty in the DSD parameters and rain dynamics.

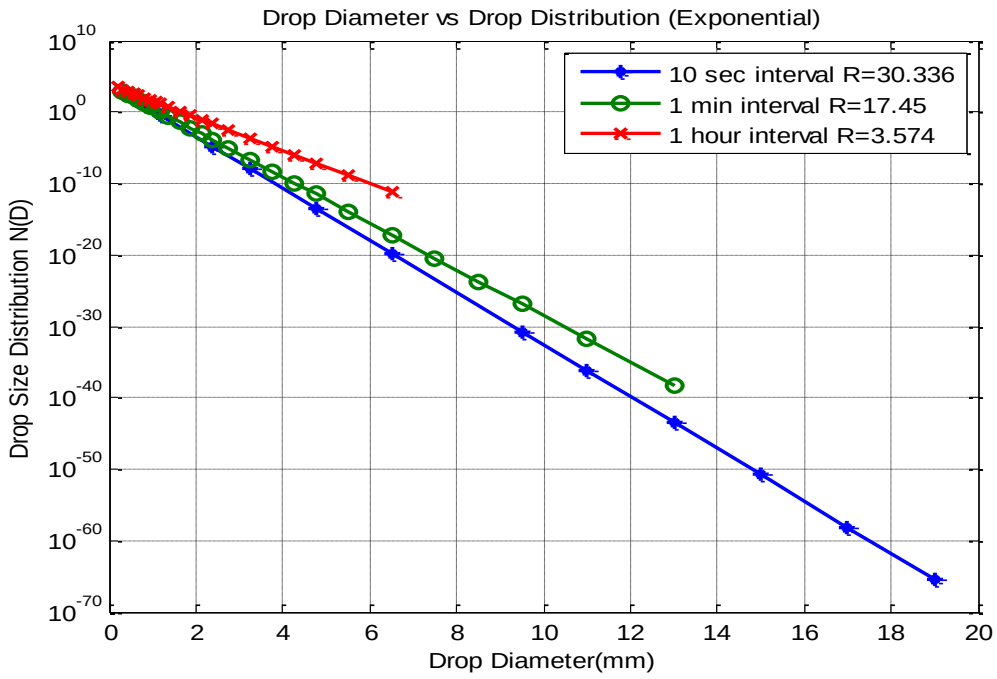

Figure4.5 Exponential drop size distribution for various rain events with different integration periods

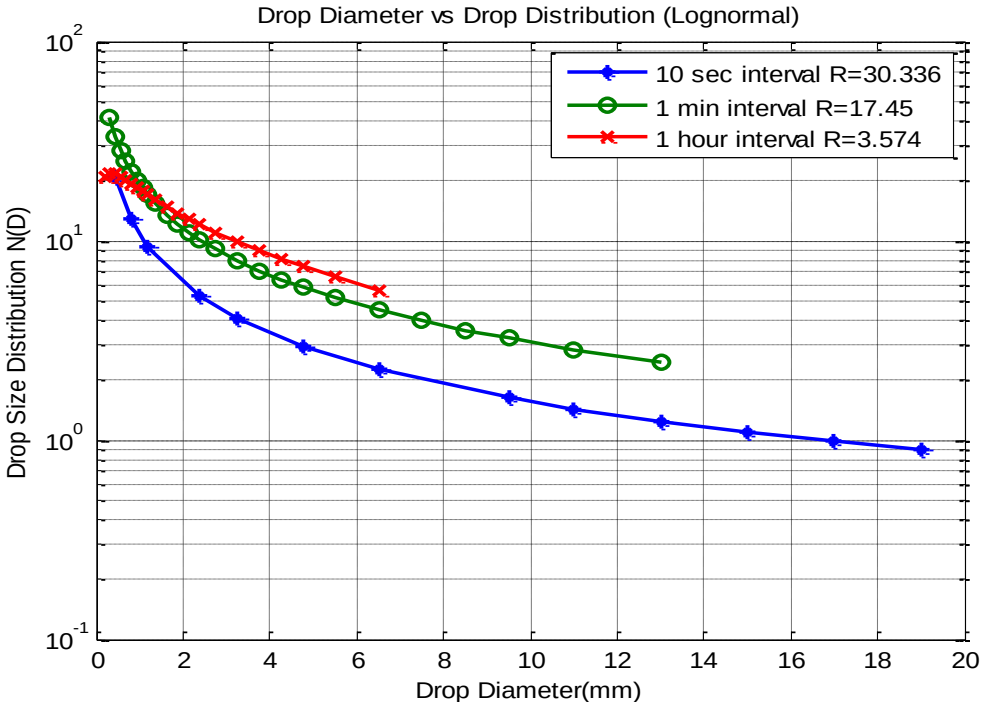

Figure4.6 Lognormal drop size distribution for various rain events with different integration periods

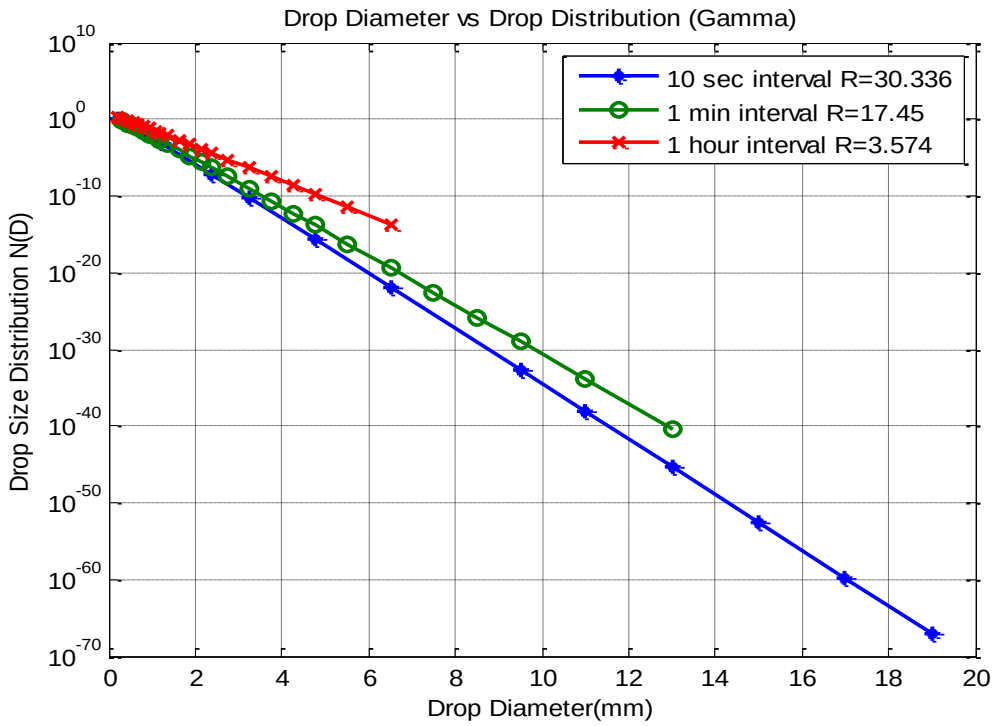

Figure4.7 Gamma drop size distribution for various rain events with different integration periods

4.5 Disdrometer Results

4.5.1 Cumulative Distribution of Rainfall Rate

Figure 4.8 shows the cumulative distribution function of rainfall intensity for OTT parsivel disdrometer data and Rec. ITU-R P.837-6 [67] and ITU-RP.618-11[70]. Disdrometer data is broadly consistent with P.837-5[67]. India is subject to regional climates, where the north part of India is mainly influenced by the Himalayas. and south Indian region is exposed to continental tropical air masses, which is mostly warmer and drier air. The inferred average cumulative distributions of rain rate over the two-year period for the experimental region are shown in Figure 4.8. The rain rates were plotted for other percentage of time 0.001% to 0.1%, of an average year. This corresponds to 5.26 minutes to 8.76 hours of exceedance of the indicated one-minute rainfall rates in an average year. It is seen that the selected region had the highest cumulative distribution of 2 to 156mm/h.

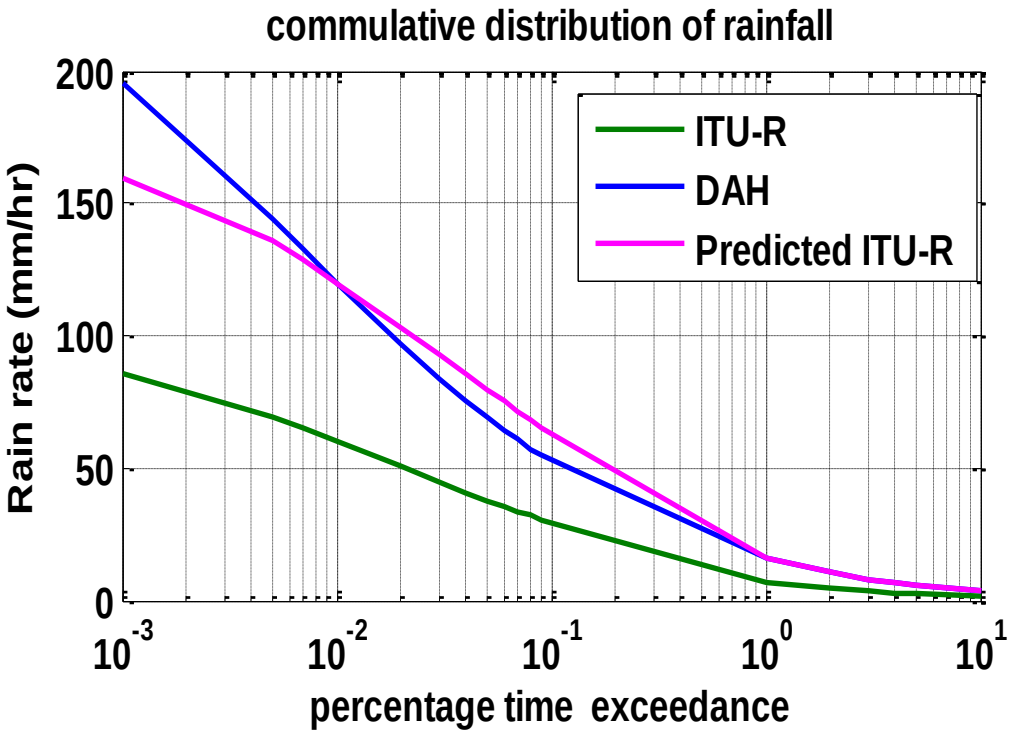

Figure4.8 Commulative distribution function of rain fall

4.5.2 Variability of DSD as a function of Rain fall rate and time

Figure 4.9 explains particularly about the variation of drop size distribution as a function of time. In all the three models the interval is taken as 10 sec interval, 1minute interval and 1 hour interval. In exponential method of distribution the rate of change of DSD with drop diameter is very low for higher integral periods; gamma distribution almost fallows the exponential distribution. In lognormal distribution the curve which represents the 1 hour interval DSD is under the remaining two curves which are for lower integral period.

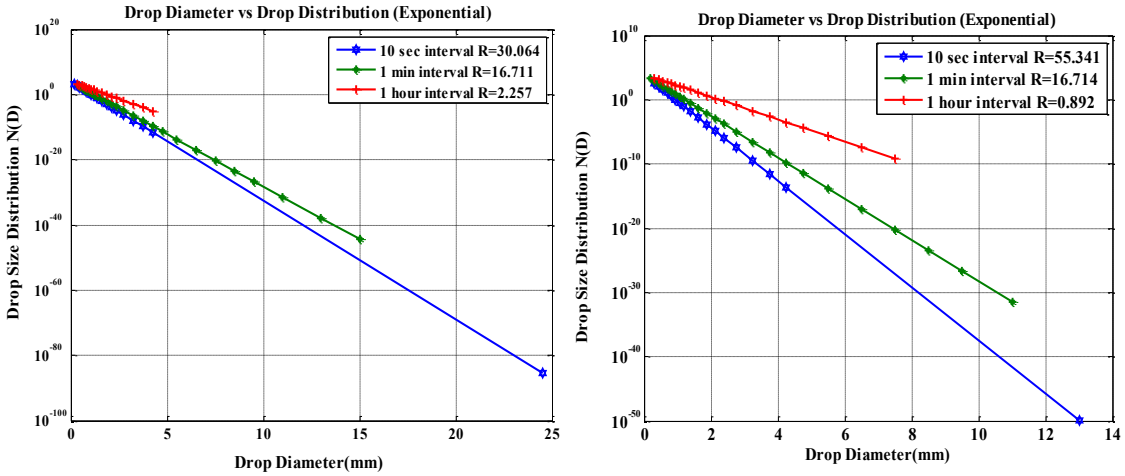

(a)

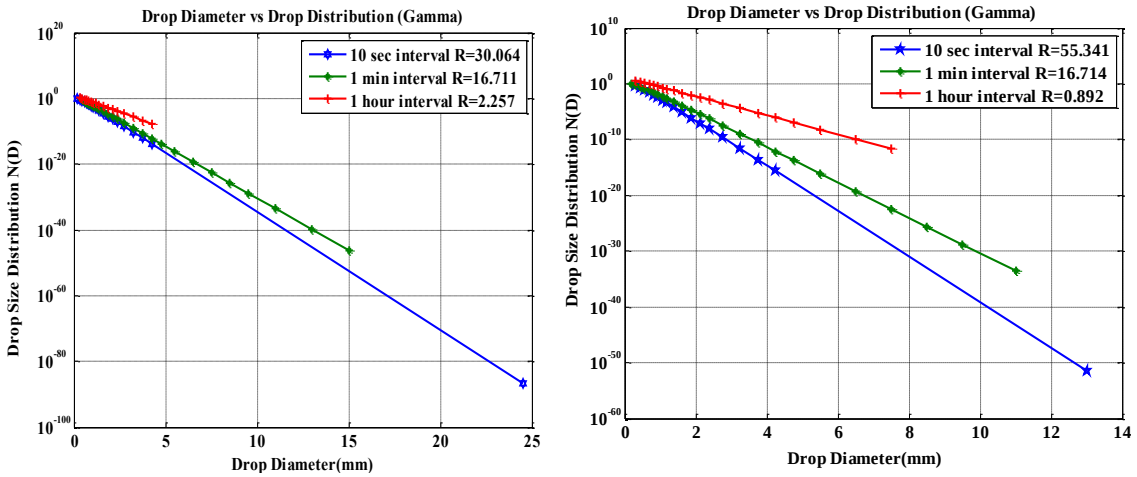

(b)

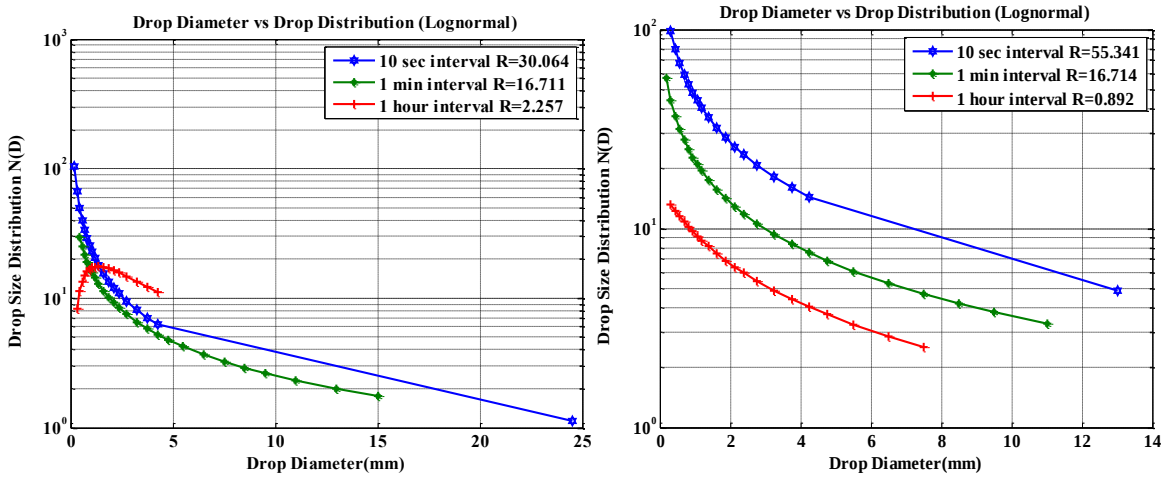

(c)

Figure: 4.9: variation of DSD as function of rain fall and time(a) using exponential distribution,(b)gamma, (c)Lognormal distribution

Figure 4.10 clearly shows the variation of DSD with rain fall using the same three methods (Exponential, Gamma, and Lognormal) for different rain fall values ranges from very small value to larger one. In exponential method the DSD decays exponentially, when the rain fall value is small it decays slowly than with higher rainfall rates. same thing was happened in gamma distribution also.DSD variation in case of lognormal distribution is different from the previous two models i.e., for lower rain fall rates curve start from lower values, for higher rain fall rates it varies almost as a straight line

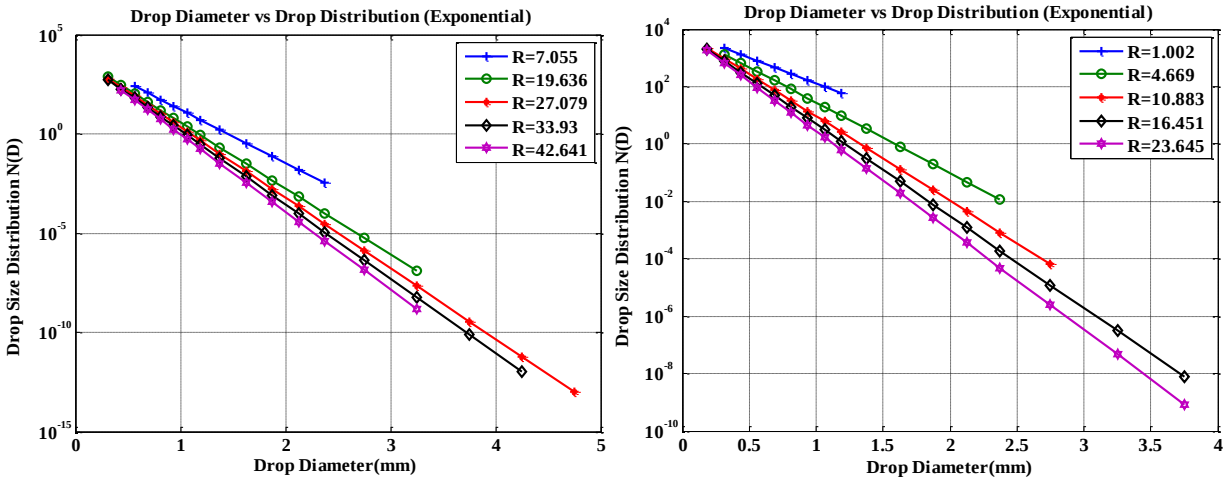

(a)

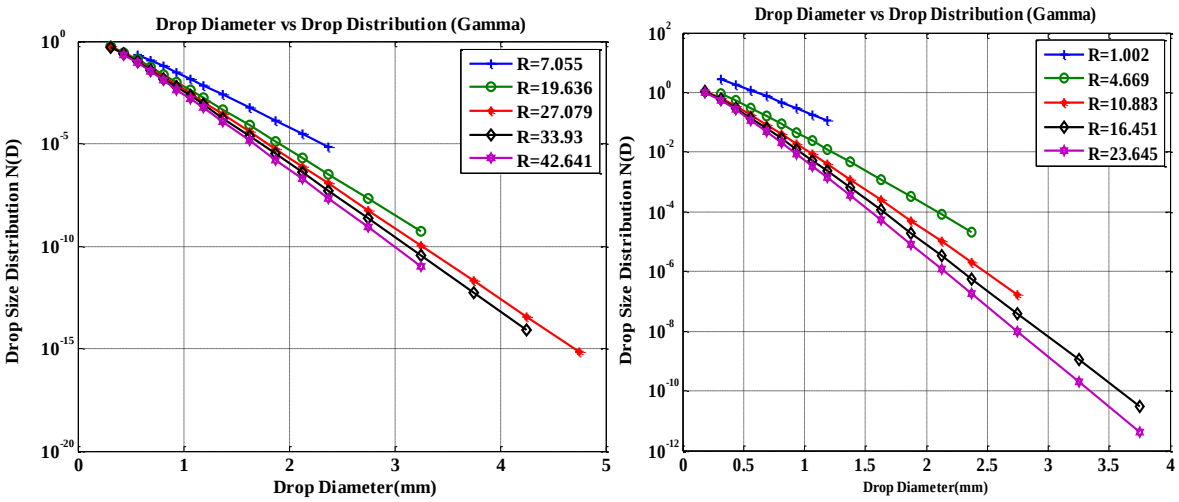

(b)

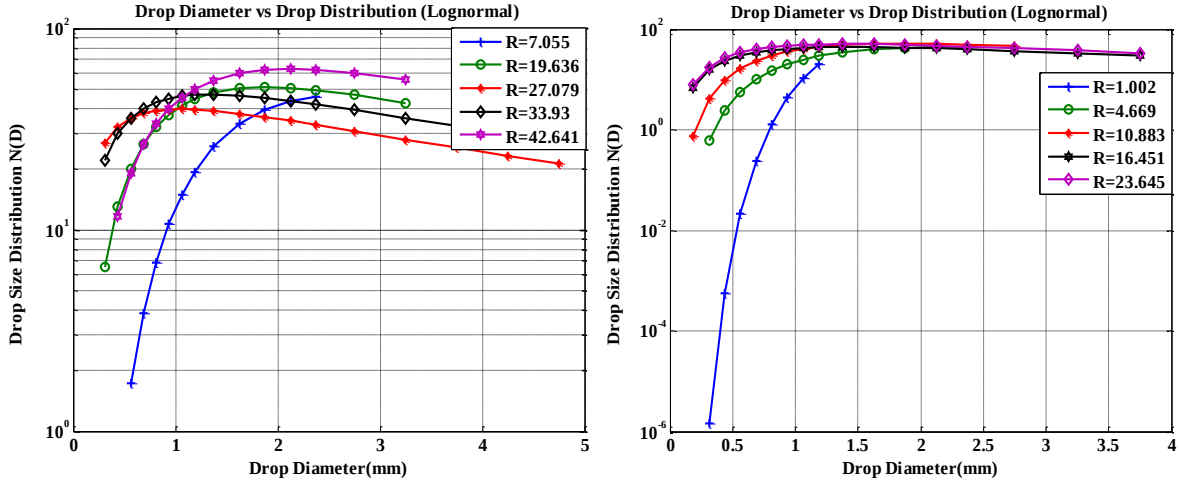

(c)

Figure: 4.10: DSD variation as a function of rain fall variation using three distribution models (a) Exponential (b) Gamma (c) Lognormal.

4.5.3 Seasonal variation of DSD

Figure 4.11 shows the variation of DSD as function of rain fall rate. The data was partitioned in to seasons; summer(March, April, May, June),winter(November, December, January, February), monsoon(July, August, September, October).figure 4.11.1 shows the lognormal distribution for three different seasons for the same rain fall. In rainy period the size of the drop concentrates only around 0mm to 4mm, in summer the concentration of drop size between 0 to 5mm and for winter drop size is in between 1mm to 19mm.in winter drop size variation is huge and the DSD also varies all most in exponentially decaying manner.

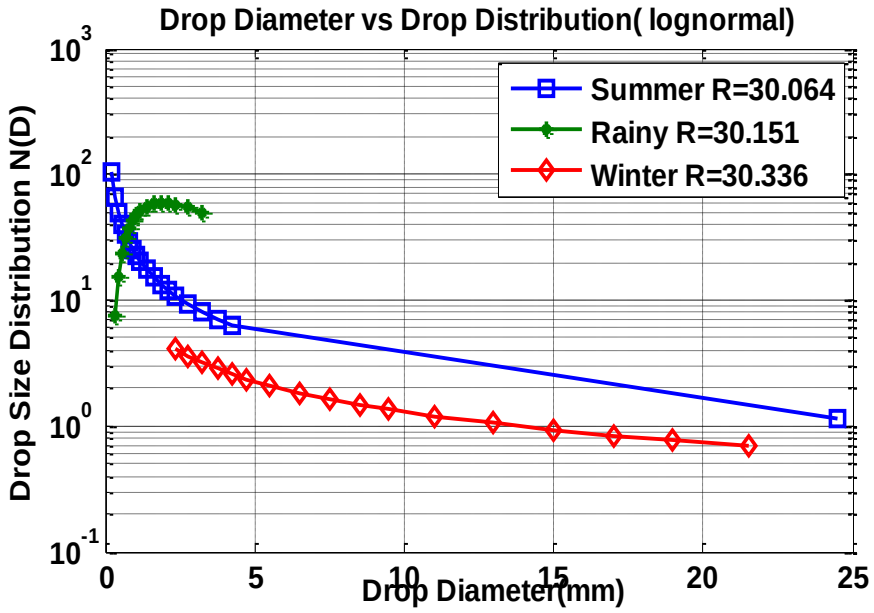

Figure 4.11.1: Variation of DSD on seasonal wise using lognormal distribution

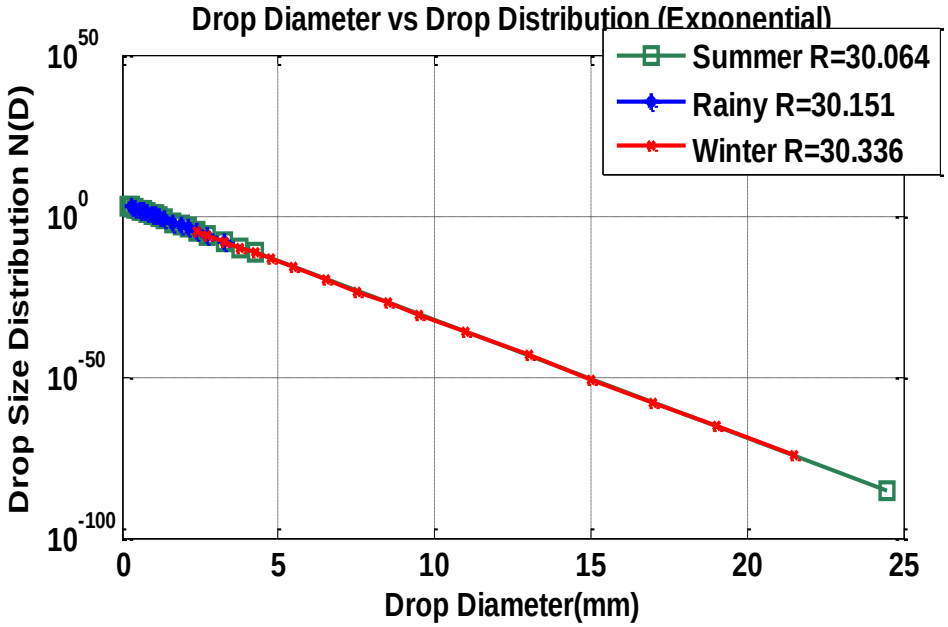

Figure 4.11.2: Variation of DSD on seasonal wise using Exponential distribution

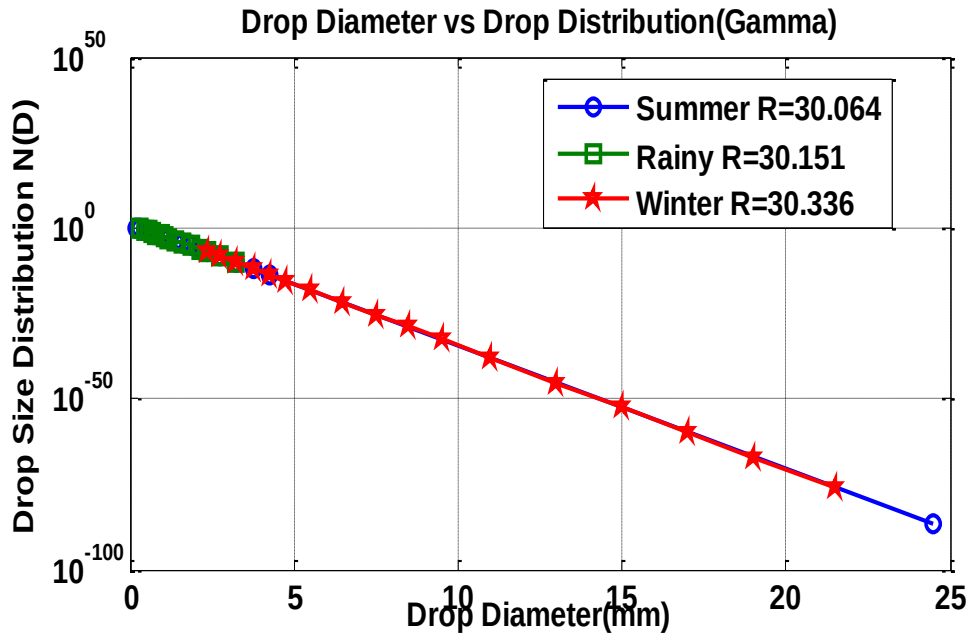

Figure 4.11.3: Variation of DSD on seasonal wise using Exponential distribution

4.6 RAIN ATTENUATION

Radio waves at EHF and SHF are susceptible to the effects of the troposphere such as gaseous absorption, cloud attenuation, increased apparent noise temperature, scintillation and, most importantly, attenuation due to rain. Rain has the most significant effect on a satellite signal especially at extra high frequencies.

4.6.1 Electromagnetic Scattering and Absorption

Attenuation on communications links is caused by the scattering and absorption of electromagnetic waves. A plane wave incident on a raindrop (Ei) induces a transmitted field in the interior of the drop and a scattered field. (Es) denotes the electric field of the scattered wave in the far field region.

$$E_s = f(\ \hat{K}1, \hat{K}2)\frac{\exp(ikr)}{r}E_i \qquad (4.14)$$

where k = 2π/λ, is the free space propagation constant, λ is the incident wavelength, r is the distance from origin of the observation point, Ei is the electric field of the incident

wave, f(K_1,K_2) is a matrix function denoting scattering amplitude and the polarization state of the scattered wave, which is obtained from the solution of the boundary value. Therefore the scattering amplitude is a function of K^1, K^2, the frequency, size, shape and material of the raindrop, and the polarization of the incident wave. The raindrop and fields are shown graphically in Figure 4.12.

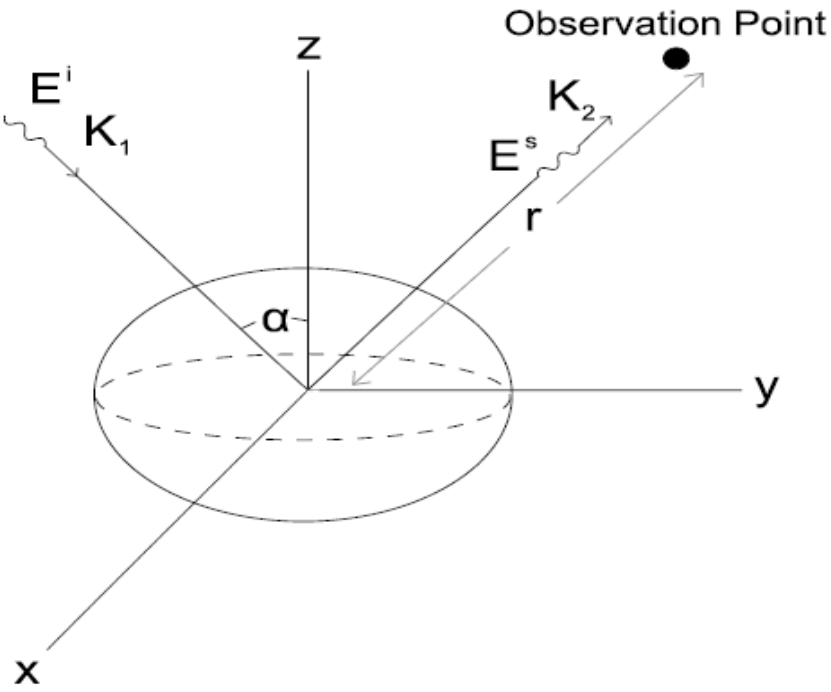

Figure4.12: Electromagnetic scattering geometry.

A hydrometeor that has a physical cross section has an absorption, scattering and total attenuation cross section[103][104][105]. The absorption cross section, Q_a, is equivalent to the power absorbed by the hydrometeor, the scattering, Q_s, is equivalent to the power scattered in all directions and the total cross section, Q_t, gives the total power removed by the hydrometeor.Q_t is directly related to attenuation of the transmitted signal, and is given by the relationship:

$$\boldsymbol{Q_t = -\left(\frac{4\pi}{k}\right) lm[\,\mathbf{e\hat{}(K\hat{}1, K\hat{}1)}]} \tag{4.15}$$

where e^ is a unit vector of the polarization state. Note that, in this case the investigation is only concerned with forward scattering, therefore K^1 = K^2. The absorption and scattering can be modelled by several different methods depending on the frequency of the signal and the shape of the drop. Example methods include the use of Rayleigh theory, Mie theory and the T-matrix. The Rayleigh method applies to frequencies lower than those considered in this research. Mie theory assumes that the shape of the raindrop is spherical, which is not the case for raindrops above 2mm in diameter. The T-matrix can model asymmetric particles, which improves the representation of a raindrop and hence increases the accuracy of attenuation estimates.

4.6.1.1 Mie Theory

Once an electromagnetic incident field is intercepted by a raindrop, the electric field induces an internal field and a scattered field. In this work, only the far fields are considered, since the near-field components are only significant up to a few wavelengths from the article. Each particle is assumed to be a homogeneous sphere and the incident field is assumed to be a plane wave.The calculation of the total extinction cross section, Qt, begins with the knowledge of the incident field. There are three expressions for the incident, internal and scattered field[105]. These equations are shown in (4.16)-(4.18) respectively.

$$\mathbf{E^1(k_r) = E_o \sum_{n=1}^{\infty} i^n \frac{2n+1}{n(n+1)} (M^1_{o1n} - iN^1_{eln})} \tag{4.16}$$

$$\mathbf{E^{int}(mkr) = E_o \sum_{n=1}^{\infty} (C_{01n} M^1_{01n} + d_{eln} N^1_{e1n})} \tag{4.17}$$

$$\mathbf{E^s(k_r) = E_o \sum_{n=1}^{\infty} \frac{2n+1}{2[n(n+1)]^2} (f_{oln} M^3_{oln} + g_{cln} N^3_{eln})} \tag{4.18}$$

where c_{o1n}, d_{e1n}, f_{o1n}, g_{e1n} are unknown internal and scattered field expansion coefficients. M^1_{o1n} and N^1_{e1n} are vector spherical harmonics of the first kind and M^3_{o1n} and N^3_{e1n} are of the third kind. Using calculations based on Mie theory, and assuming the object is a sphere, the expansion coefficients can be calculated in closed form. The internal field and scattered field coefficients are calculated in terms of spherical triple indexes σ, m, n and size parameter x = ka, where a is sphere radius and k is the wave number.

Using equations (4.15) and (4.18) [105] shows how the total cross section, Qt, can be calculated. Qt can be expressed in the form of equation (4.19) [103].

$$\boldsymbol{Q_t = -\left(\frac{2\pi}{k^2}\right) Re[\sum_{n=1}^{\infty}(2n+1)(a_n^3 + b_n^3)]} \qquad (4.19)$$

The values of $\boldsymbol{a_n^3}$ and $\boldsymbol{b_n^3}$ are the expansion coefficients according to a spherical elementary solution.

4.6.1.2 T-Matrix

The T-matrix is ideal for calculating scattering by asymmetric dielectric particles, which is the typical shape of a raindrop. One method to calculate specific attenuation uses the normalized extinction cross section, which can be determined by the T-matrix [103]. The normalized extinction cross section is given by (4.20).

$$\mathbf{Q_t = \frac{4\pi}{k_v^2} lm(e_o, kF)} \qquad (4.20)$$

where F is the vector far-field amplitude, k_v is the wave propagation vector, e_o is a unit polarization vector multiplied by a unit vector in the direction of propagation and $k = 2\pi/\lambda$.

$$\boldsymbol{E^s = F\frac{\exp(ik_{vr})}{r} E_i} \qquad (4.21)$$

T-matrix method begins by the expansion of the incident, scattered and internal electric fields in terms of spherical harmonic functions[105].

The T-matrix provides a more accurate estimate of Qt for elliptical shape raindrops and hence an improved determination of specific attenuation compared to Mie theory. Waterman [106], Barber and Hill [105] and Ishimaru [107] have provided further details on solving the expansion coefficients and using the T-matrix method.

4.6.2 Specific Attenuation

The specific attenuation describes the attenuation of a radio wave per unit distance. The specific attenuation is a function of the total cross section of a raindrop, Qt. In this work, Qt is calculated using the T-Matrix method with the drop shape model [108] .It is important to consider that the calculations are dependent on temperature, drop shape model, drop fall velocity model [32] and the method of scattering function calculation. Assuming a plane wave propagating in a rainy medium, the governing equation of variation of wave intensity is given by

$$\frac{dI}{dz} = -(\sum Q_t)I \qquad (4.22)$$

Where ∑Qt is the sum of the total cross sections of all the raindrops in a unit volume in space. Equation (4.22) implies the rate of decrease of wave intensity in a thin slab of thickness dz proportional to the energy absorbed and scattered by the raindrops within the slab. Integrating,

$$I = I_o \exp(-(\sum Q_t)z) \qquad (4.23)$$

where I_0 is intensity at z = 0. The sum of the total cross sections in an area da can be calculated as shown in equation (4.24).

$$\sum Q_t = \int Q_t(D)N(D)dD \qquad (4.24)$$

Considering Qt and intensity, specific attenuation is given by equation (4.25)[103].

$$A = 4.344X10^3 X \int Q_t(D)N(D)dD \qquad (4.25)$$

4.6.3 Multiple Scattering

Multiple scattering has not been considered when calculating specific attenuation. A radio wave scattered by a raindrop will leave in multiple directions, which could then be scattered through another drop and redirected towards a receiver. multiple scattering causing incoherent waves has little impact on satellite links and

should only become an issue for frequencies greater than 300GHz[109][110]. Therefore multiple scattering has not been considered in this thesis.

4.6.4 Polarization

Specific attenuation not only depends on frequency but also on polarization [113]. Electromagnetic wave polarization describes the orientation of the wave oscillations. There are several types of polarization, including linear polarization (vertical and horizontal), circular and elliptical polarizations. The polarization of the electromagnetic signal alters the manner in which a raindrop scatters the signals and thus effects the specific attenuation. Figure 4.14 shows the effects of polarization on specific attenuation at frequencies of 10-55GHz for 10mmh^{-1}, 20mmh^{-1}, 30mmh^{-1}, 50mmh^{-1}, 90mmh^{-1} and 120 mmhr−1. The specific attenuation was calculated based on the Marshall and Palmer exponential DSD model [63] equation (4.2), and assuming a terrestrial link with horizontal elevation. These results show the difference between vertical and horizontal

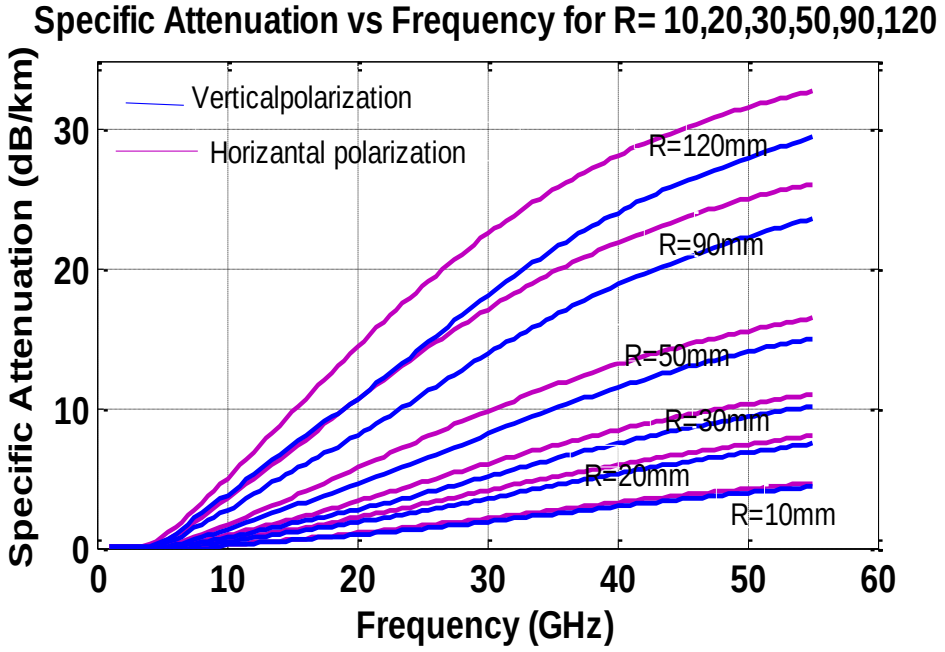

Figure 4.13: Specific attenuation for horizontal and vertical polarization plotted against Frequencies from 0 to 55Ghz.

specific attenuation is relatively small, especially at low rainfall rates (e.g., 5mmhr^{-1}).Typically, at low rainfall rates the mean drop size Dm is relatively small (below 2mm diameter)[111]. Raindrops below 2mm diameter can be considered approximately spherical; hence the effect of polarization is minimal [112].

4.6.5 Variability in the Attenuation and Rain Fall Rate Relationship

In this section of analysis, to observe the effects of attenuation for different frequencies ranging from 10 to50 GHz. Particularly discusses about the frequency of 11.7GHz due to the availability of beacon data used to validate estimates of the attenuation rainfall rate relationship. Further consideration of the effect of frequency and polarization are already discussed. Figure 4.14 shows the variability in the attenuation rainfall relationship for two and half years of data from Ott parsivel Disdrometer collected between June 2012 and October 2014.

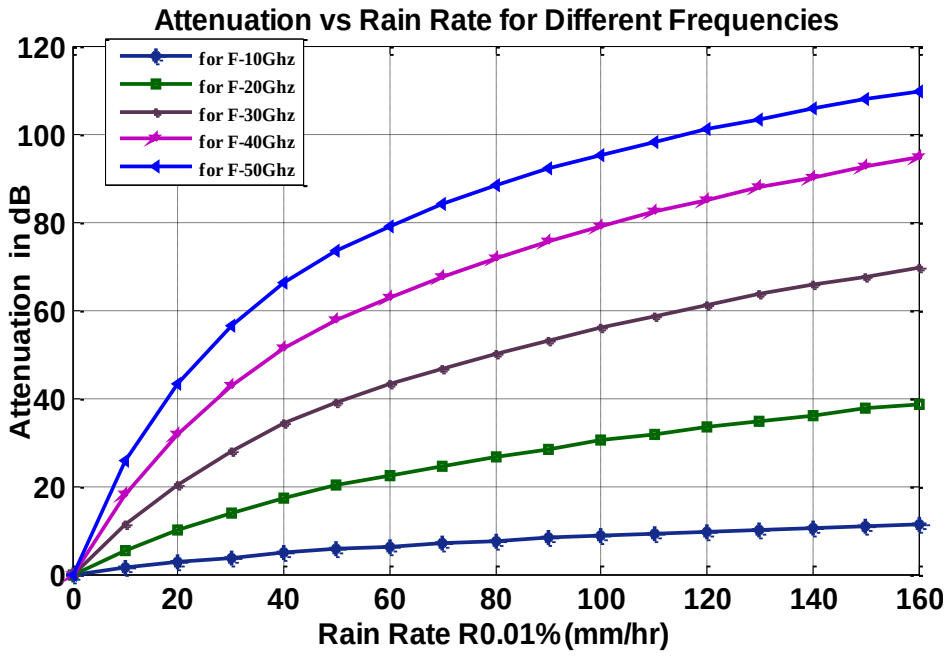

Figure 4.14: attenuation variation with rainfall rate for both vertical and horizontal polarization

For frequencies below 20 GHz Attenuation for lower rain fall was increased linearly with the increase of rain fall, for heavy rain fall the rate of increment in attenuation is less than at lower rain fall. For frequencies which are above 20 GHz, the increment in attenuation with R value is following the square law behaviour. In chapter V attenuation calculation using different models is going to be discussed.